npj | climate and atmospheric science

www.nature.com/npjclimatsci

ARTICLE OPEN

Check for updates

Influence of monsoon low pressure systems on South Asian disasters and implications for disaster prediction

D. L. Suhas[1]✉, Nandini Ramesh[2], Ram M. Kripa[1] and William R. Boos[1,3]

Transient atmospheric vortices called monsoon low pressure systems (LPS) generate a large fraction of total rainfall over South Asia and often produce extreme precipitation. Here, we assess the influence of these storms on the occurrence of disasters, using information from the Emergency Events Database (EM-DAT) that we geocoded and then associated with LPS tracks. We show that more than half of hydro-meteorological disasters over South Asia during summer are associated with these LPS events. Weaker LPS (which are called monsoon lows) occur more frequently than stronger LPS (called monsoon depressions), but the stronger LPS produce a larger number of disasters. Furthermore, although many prior studies have shown that the peak rainfall in LPS falls southwest of the vortex centre, the disasters are concentrated on the northern edge of the LPS tracks, along the Himalayas and upper basins of the Ganga and Brahmaputra rivers. Observations show a sharp peak in rainfall on the day of disasters, confirming the physical link between LPS and these hydro-meteorological disasters. A similar peak in rainfall is found in weather forecasts made up to five days before the disaster, suggesting that short-term precipitation forecasts can be useful in disaster preparation.

npj Climate and Atmospheric Science (2023)6:48 ; https://doi.org/10.1038/s41612-023-00376-5

INTRODUCTION

Globally, natural disasters affect many millions of people each year and cause tens to hundreds of thousands of deaths annually[1,2]. While the frequency of disasters seems to have increased over the last few decades[3,4], improvements in warning systems and mitigation strategies have reduced some of their impact[5–8]. This motivates efforts to not only understand the factors responsible for disasters, but to better forecast and prepare for these events.

South Asia is especially vulnerable to natural disasters, due to its abundant meteorological and seismic hazards, its high population density, and its lower level of economic development[6,9]. Floods and storms are especially prominent in South Asia, producing 60–80% of the total number of natural disasters there[10,11]. Compared to geological disasters, such hydro-meteorological disasters also have a higher risk of transforming into a large-scale catastrophic disaster[4,12].

Monsoon low pressure systems (LPS) are the principal rain-bearing systems observed over South Asia during boreal summer, forming and propagating within the larger, continental-scale monsoon circulation. These atmospheric vortices have a horizontal scale of about 2000 km and last for about 3–6 days[13,14]. They form most often over the Bay of Bengal and propagate northwestward, with peak precipitation falling southwest of the vortex centre[15,16]. Individual LPS are typically classified as weaker monsoon lows or stronger monsoon depressions, based on the strength of their winds[17–19]. The total population of LPS is collectively responsible for a large fraction of monsoonal precipitation over South Asia[13,20,21], and individual LPS are often associated with extreme rainfall events[18,22,23]. A recent study showed that over 80% of the extreme precipitation events over Central India occur on days when an LPS exists[24].

While many studies have explored the association between monsoon LPS and extreme precipitation events[18,24,25], none have yet determined how many natural disasters in South Asia are caused by LPS and their associated rainfall. This task is undertaken here. Specifically, we geocode hydro-meteorological disasters in South Asia from a mass-casualty disaster dataset, then associate these with LPS tracks obtained from an automated tracking algorithm applied to atmospheric reanalysis data[19]. We examine the geographic distribution of these disasters along with the associated time series of rainfall. We also briefly analyze the skill of short-term forecasts of past rainfall associated with disasters, and discuss the utility of such forecasts in disaster preparation. The results are presented in "Results" and conclusions are provided in "Discussion". Data and methodology employed in our study is outlined in "Methods".

RESULTS

Disaster association with LPS tracks

According to EM-DAT, South Asia has experienced 344 disaster events, affecting 2394 disaster locations during June to September of 1990–2019 (Table 1). More than 90% of these disaster events are of hydrological or meteorological origin. On associating the hydro-meteorological disasters with LPS tracks, we find that more than half of the disaster events can be tied to LPS (Table 2). Here, we associate the disaster event with an LPS if at least half of the disaster locations constituting a given disaster event are within 800 km of the LPS track. More details regarding this are discussed in the "Methods" section. One important result can be noted immediately: although monsoon lows occur more frequently than depressions, the depressions are responsible for more disasters. There is some overlap between the lows and depressions, as a single disaster event can be associated with multiple LPS; this is why the sum of the disaster events associated with lows and those associated with depressions is about 25% larger than the number of events associated with all LPS.

There is a spatial offset between the regions of peak LPS track density and the regions in which LPS-related disasters are most frequent. The precipitation associated with monsoon LPS has a

[1]Department of Earth and Planetary Science, University of California, Berkeley, USA. [2]Natural Systems Modelling Group, Data61, Commonwealth Scientific and Industrial Research Organisation, Canberra, Australia. [3]Climate and Ecosystem Sciences Division, Lawrence Berkeley National Laboratory, Berkeley, USA. ✉email: suhasdl@berkeley.edu

peak over central and western India, with heavy rainfall also observed over eastern India and the foothills of the Himalayas[24]; this is consistent with the location of LPS tracks (brown lines in Fig. 1a). In contrast, the hydro-meteorological disasters associated with monsoon LPS are mostly concentrated along the Himalayas and the upper basins of the Ganga and Brahmaputra rivers, with a substantial number also present in other river basins (red dots in Fig. 1a). In fact, about 60% of these disasters are due to riverine floods, according to EM-DAT, and such floods can be caused by both local and upstream rainfall, with some temporal offset. For example, the Ganga and Brahmaputra basins are over 1000 km in horizontal extent, and it can take three weeks for water to travel from the uppermost parts of those basins to the river mouth[26]. Our analysis does not account for large temporal offsets between LPS precipitation and resulting floods, but given typical LPS propagation speeds of 2–3 ms^{-1} and the 800 km radius we use to associate a disaster with an LPS, this allows for about four days of offset between the peak precipitation near the centre of a typical LPS and the occurrence of a disaster. Larger temporal and spatial offsets between precipitation and flooding are expected to shift disasters relative to precipitation for some of the riverine floods; these are not included in our analysis, but a relevant example is discussed in "Precipitation forecast skill".

Table 1. Summary of the EM-DAT dataset for disasters over South Asia during June–September 1990–2019.

Description	Count
Total disasters	344 (2394)
Hydrological	286 (2219)
Meteorological	31 (105)
Geophysical	12 (44)
Biological	15 (26)

The number of disaster events is shown for each category, with the number of disaster locations in parentheses. Here, the disaster event refers to a single large-scale event, while the constituent locations affected by it are referred to as disaster locations.

Table 2. Numbers of hydro-meteorological disaster events and subsets associated with LPS.

Description	Count
Hydro–meteorological disasters	317
Disaster events associated with LPS	180
Disaster events associated with depressions	129
Disaster events associated with lows	103
Disaster events associated with both depressions and lows	52
Number of depressions	201
Number of lows	304

The sum of disaster events associated with depressions and lows is larger than the number associated with LPS because the same disaster event can be associated with multiple LPS. The number of depressions and lows refer to the count over the domain 0°N–40°N and 50°E–100°E, during June–September of 1990–2019.

A storm-centred composite of disaster frequency confirms that the disasters associated with LPS predominately lie along the northern edge of the LPS tracks (Fig. 1b). This is true even though the peak precipitation in LPS is well-known to typically fall southwest of the vortex centre[13,27,28] (Supplementary Fig. 1). Since disaster risk depends on human exposure and vulnerability, as well as geomorphic factors that control the likelihood of a given rainfall event to produce a flood[29], this spatial offset may result from a number of factors. One important factor is the large human population density[30,31] along the Ganga and Brahmaputra river basins (Supplementary Fig. 2a). The peak population lies mostly to the north of the LPS tracks, which can also be seen in an LPS-centred composite of population density (Supplementary Fig. 2b). This alone shifts the human exposure to LPS rainfall northward relative to the LPS tracks. Geomorphic factors may also be responsible for shifting the frequency of disaster occurrence toward Nepal, as the Himalayas are prone to floods and landslides during extreme precipitation events[32,33].

We now test whether the association between LPS and disasters may occur by chance, determining how much the presence of an LPS raises the probability of disaster occurrence. The geographic distribution of disaster frequency is shown in Fig. 2a, in terms of the total number of disaster locations occurring in individual 2°×2° subregions during June–September of 1990–2019. As in Fig. 1a, the disasters remain concentrated mainly along the Himalayas and upper basins of the Ganga and Brahmaputra rivers, with parts of those regions experiencing more than 100 disasters per 2°×2° subregion over the time span considered (note the

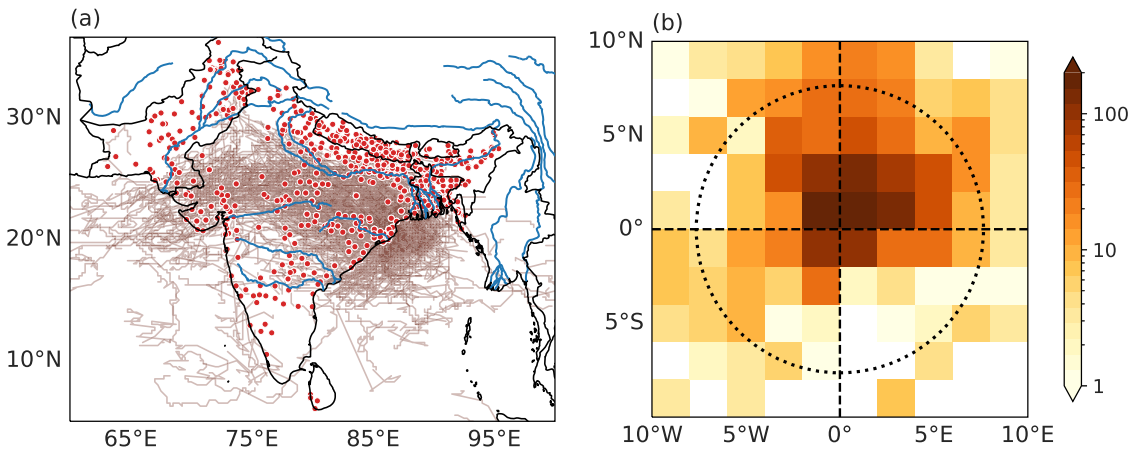

Fig. 1 Spatial distribution of disasters. a The location of hydro-meteorological disasters (red circles) associated with monsoon LPS and the tracks of LPS (in brown), during June–September of 1990–2019. Only the tracks of LPS associated with disasters are shown. Major rivers are shown in blue. **b** The location of disasters relative to the LPS centre. The relative distance is computed at the time of minimum separation between the disaster location and LPS centre. Black dashed circle indicates the 800 km radius (at 20°N), that is used to associate disasters with monsoon LPS.

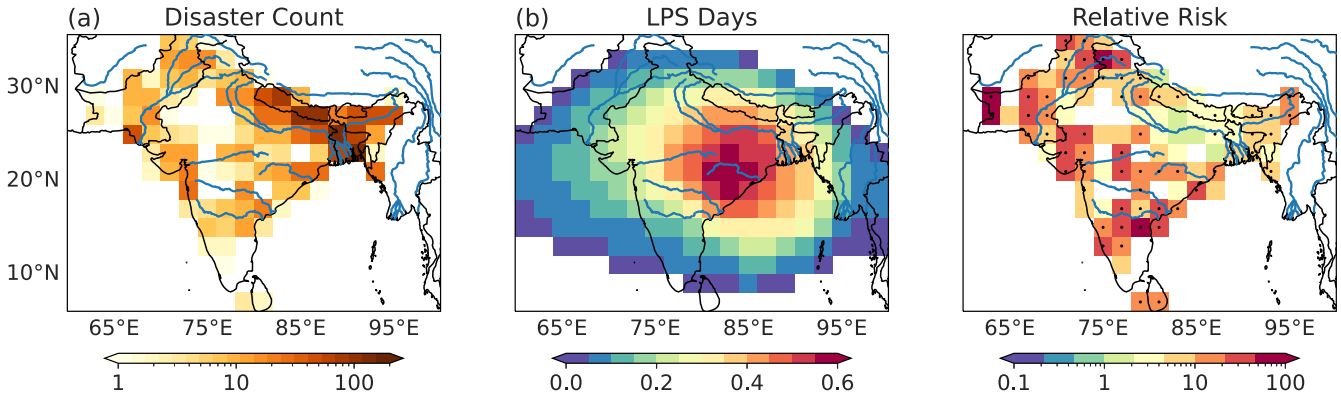

Fig. 2 Association of LPS with disaster occurrence. a Number of disaster locations associated with monsoon LPS, **b** fraction of days in the June–September season on which the region is under the influence of LPS (i.e. within 800 km of an LPS track) and **c** the relative risk of disasters due to the presence of LPS, all in individual 2°×2° subregions. Relative risk >1 indicates that the risk of occurrence of disasters is increased due to the presence of LPS. Stippling indicates the region where the 95% confidence interval of relative risk is above the value 1. The plots are computed for June–September of 1990–2019.

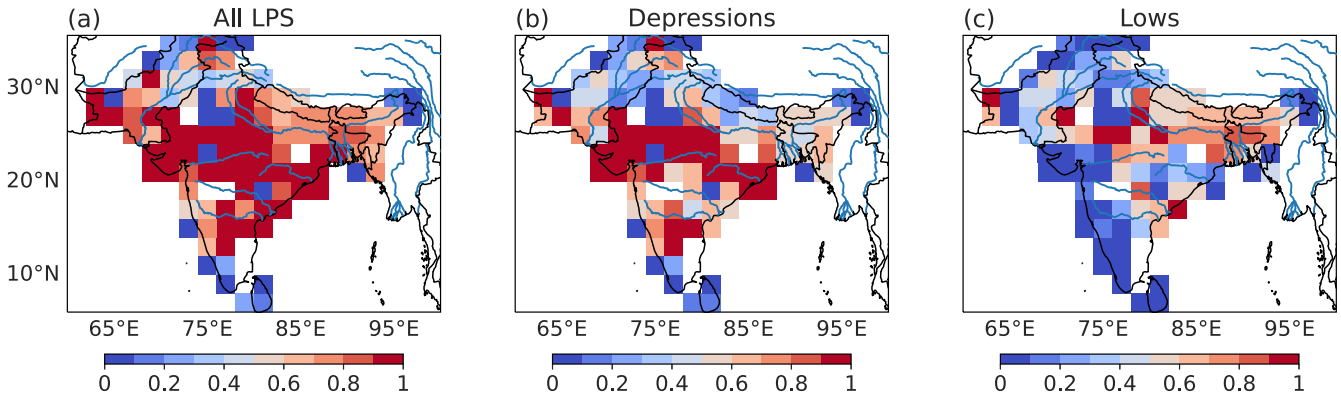

Fig. 3 Fraction of disasters associated with LPS. The fraction of disaster locations associated with **a** all LPS, **b** depressions, and **c** lows, during June–September of 1990–2019.

logarithmic colour scale). The fraction of days for which each 2°×2° subregion is under the influence of LPS (meaning that the region lies within 800 km of an LPS centre) is shown in Fig. 2b. The peak occurs over eastern India, where about 50–60% of days in June-September are under the influence of LPS. However, the rest of South Asia, including regions with the highest frequency of disasters like the foothills of the Himalayas, are under the influence of LPS for less than half of the monsoonal season. The relative risk, defined as the ratio of the probability of occurrence of disasters during LPS events to the probability of disasters in the absence of LPS, is shown in Fig. 2c. Relative risk >1 indicates that the risk of disasters is increased when LPS are located within 800 km of the grid cell[34]. Most of the domain has a relative risk much greater than 1, with many of the grid points being statistically significant, as inferred from the 95% confidence interval of relative risk being above unity[35].

We next examine the fraction of disasters associated with stronger and weaker LPS (depressions and lows, respectively). The fraction of disaster locations associated with all monsoon LPS in each of the individual 2°×2° subregions is shown in Fig. 3a. Over a large part of the domain, more than half of the disaster locations are associated with LPS, even though these regions are under the influence of monsoon LPS for <50% of the monsoonal season (Fig. 2b). This is consistent with our relative risk calculation above. The contribution of monsoon depressions is above 50% over most of the domain, while disasters associated with lows are more concentrated over Nepal, Bhutan, and northeastern India as well as along the Ganga and Brahmaputra river basins (Fig. 3b, c), as these regions experience higher track density of lows than depressions (Supplementary Fig. 3).

These results have a few caveats. First, although a large fraction of disasters over central and peninsular India is associated with LPS, the number of disasters occurring over these regions is comparatively low (e.g., Fig. 1a). Second, some disasters over the west coast of India might be caused by precipitation produced by mid-tropospheric cyclones[36]; some of these disasters may be classified here as being associated with LPS because mid-tropospheric cyclones can evolve from LPS[37], and the extension of those cyclones into the lower troposphere would allow those storms to be included in our LPS dataset.

Observed precipitation

The algorithm that we used to detect LPS identified these storms using patterns of winds in the lower troposphere, so the physical link between LPS and the precipitation involved in hydrological disasters still needs to be established. Observed precipitation (from GPM) shows a peak in rainfall on the day of disasters in the composite mean (Fig. 4), confirming that physical link. Here the time series of precipitation is constructed by taking the mean rainfall within a 1° radius of each disaster location, averaging it over the locations associated with each disaster event, then taking the mean across all the disaster events. This ensures that few disaster events with a large number of affected locations do not bias our analysis. The peak rainfall occurs on the day of the disaster (day 0) and has a mean amplitude of about 30 mm/day. This is less than the typical peak LPS rainfall[38], but here we are

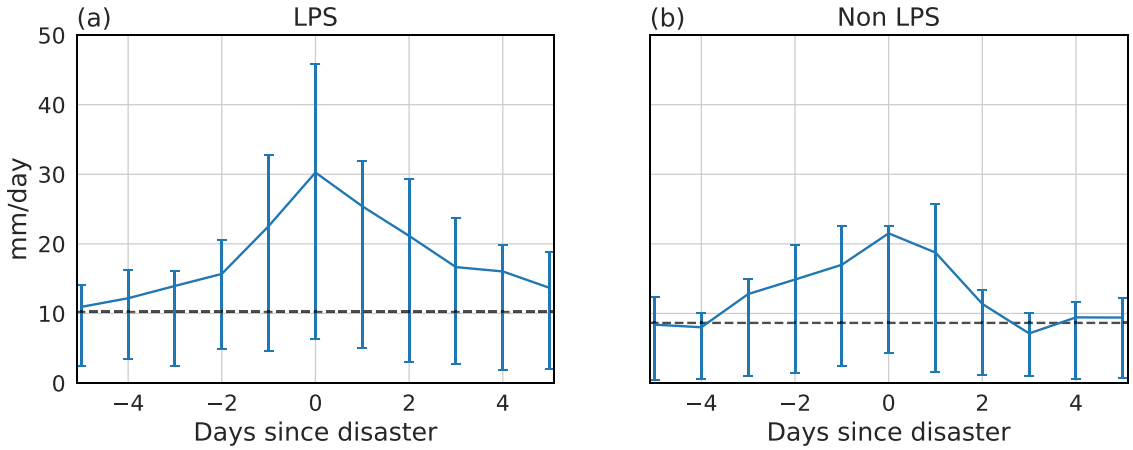

Fig. 4 Observed GPM precipitation for disaster events. Composite mean time series of observed daily rainfall (GPM) at the disaster location for the disaster events (**a**) associated with LPS and (**b**) not associated with LPS. Day 0 corresponds to the day the disaster occurs. The time series is computed by taking the mean rainfall within 1° radii of the disaster locations, first averaging over the various locations associated with a given disaster event, and then taking a mean across all the disaster events. The bars mark the 25th and 75th percentiles. The plots are for the years 2001–2019. Black dashed lines show the monthly climatological rainfall averaged over the disaster locations.

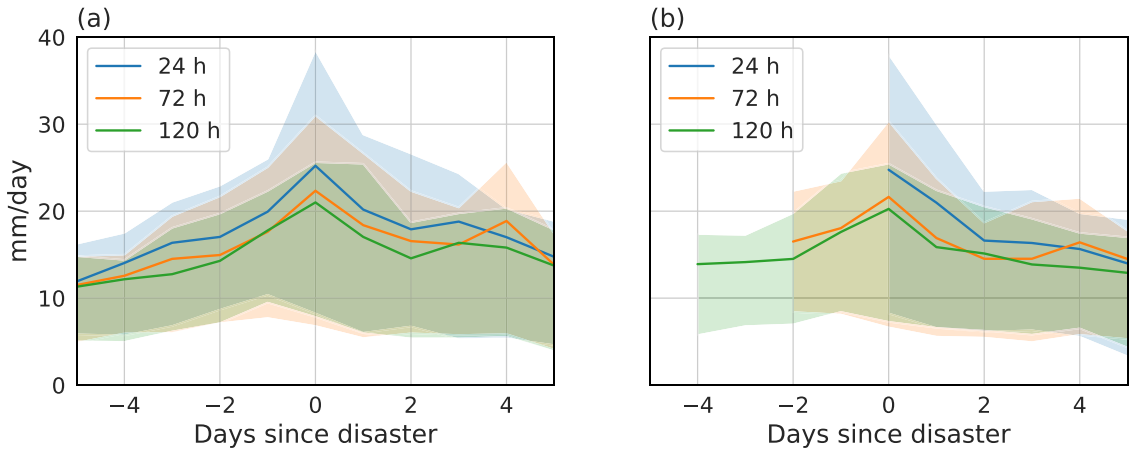

Fig. 5 ECMWF precipitation forecasts for disasters associated with LPS. Time series of ECMWF model forecast daily rainfall at the disaster location for the disaster events associated with LPS, **a** for forecasts made 24, 72, and 120 h before each day in the time series, and **b** for forecasts made 24, 72, and 120 h before the day of the disaster. Day 0 corresponds to the day the disaster occurs. The shaded region spans the 25th and 75th percentiles. The plots are for the years 2007–2019.

examining the precipitation at the location of disasters, which need not align with the location of the precipitation peak.

The mean rainfall on the day of the composite mean disaster (day 0) is about 50% higher for disasters associated with LPS than for non-LPS disasters. This suggests a physical link between LPS, the extreme precipitation produced by LPS, and the occurrence of disasters. Furthermore, peak rainfall on day 0 is higher for disasters associated with depressions as compared to those associated with lows (not shown). Since the EM-DAT dataset from which disaster locations and times are obtained contains no physical environmental variables, it is notable that these precipitation time series result from composites based only on our geocoded EM-DAT coordinates. It is also consequential that precipitation peaks on the day of disasters and not a day or two before, at least in the composite mean, and that precipitation rates are higher for LPS-related disasters.

Precipitation forecast skill

We now assess the skill with which precipitation at the location of LPS-associated disasters can be forecast. We assess this for short-term (1–5 days lead time) predictions made with the ECMWF model, as described in the "Methods" section. Figure 5a shows the time series of predicted daily rainfall for the disasters associated with monsoon LPS, with forecasts made 24, 72 and 120 hours before each day in the composite time series. Figure 5b shows a similar time series for forecasts made at various times before the day of disaster. Results from these two methods are shown to provide two distinct perspectives on the predictive skill. For example, Fig. 5a shows forecasts made 72 h before each day in the disaster time series, while Fig. 5b shows the forecast made only once 72 h before the day of the disaster. In both cases, a peak in rainfall occurs at day 0 for various forecast lead times, although the peak decreases in magnitude with increasing lead times. And similar to observed precipitation, the mean rainfall on the day of the disaster (day 0) is about 50% higher for disaster events associated with LPS than for those not associated with LPS (Supplementary Fig. 4). The predicted precipitation peak on the day of the disaster is about 20% lower than the observed peak (compare Figs. 5 and 4a). The underestimation in the ECMWF model can also be seen in storm-centred composites and a scatter plot of spatially averaged precipitation (Supplementary Fig. 1), where the ECMWF model underestimates the magnitude of peak precipitation. But the model forecasts are, if anything, slightly

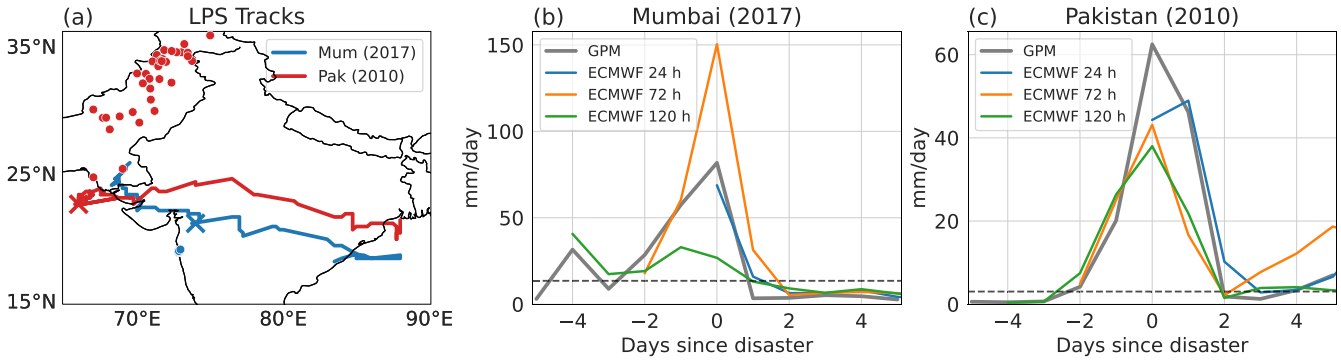

Fig. 6 Case study of two disaster events. a LPS track and disaster locations (filled circles) for the 2017 Mumbai flood and 2010 Pakistan floods. The position of the LPS at the start date of the disaster events are indicated by the crosses. Also shown are the time series of daily rainfall from GPM observations and ECMWF model forecasts at the disaster location for the **b** Mumbai and **c** Pakistan floods. The ECMWF forecasts are made 24, 72, and 120 h before the day of the disasters. According to the EM-DAT database, the flood in Mumbai started on August 29, 2017 and the Pakistan flood started on July 28, 2010. Black dashed lines show the climatological monthly mean rainfall at the location of the disasters.

underdispersive compared to the observations (as indicated by the error bars in Figs. 4 and 5), as is also seen in many of the Subseasonal-to-Seasonal (S2S) model forecasts[39]. Nevertheless, a clear peak in rainfall with forecasts made even five days before disasters suggests that short-term forecasts can be used to improve disaster warning and preparation.

We now discuss brief case studies of two well-known disaster events: flooding in Mumbai in 2017 and the 2010 Pakistan floods. The Mumbai flood was associated with a monsoon depression that had genesis over the Bay of Bengal on August 26, 2017 (Fig. 6a). It travelled westward and passed Mumbai on August 29, producing heavy precipitation near 80 mm/day (Fig. 6b). A strong precipitation peak was seen in ECMWF forecasts made up to 72 h before the disaster, although the forecast with lead time of 72 h predicted a precipitation peak nearly twice the observed magnitude; the 120-h forecast did not show intense rainfall in Mumbai.

Our second brief case study focuses on the 2010 floods in Pakistan, which occurred when a monsoon depression formed over the Bay of Bengal on July 24, 2010 and propagated westward to reach the Arabian Sea around July 28. Past work has argued that this depression combined with anomalous high pressure over the Tibetan Plateau to produce southeasterly upslope flow, moistening, and heavy precipitation over Pakistan near the Indus Valley[23]. However, as most of the EM-DAT disaster locations associated with this disaster event are further than 800 km from the LPS track (Fig. 6a), our analysis did not associate this event with monsoon LPS. We nevertheless include this case study here to illustrate some ways in which our analysis may underestimate the contribution of LPS to hydrological disasters; the effects of monsoon LPS can extend beyond the 800 km distance from the LPS track used in our attribution. Observed GPM precipitation for the 2010 Pakistan flood has a peak on the day of the EM-DAT disaster with magnitude of about 60 mm/day. The ECMWF model forecasts have a peak on the day of the disaster, even for forecasts made up to five days in advance; these forecasts underestimate the magnitude of the precipitation peak by about 30%.

DISCUSSION

Here we associated monsoon LPS with the occurrence of natural disasters in South Asia. We used geocoded disaster information from EM-DAT to associate hydro-meteorological disasters with LPS for the rainy season of June–September. The disasters are most heavily concentrated along the Himalayas and the upper basins of the Ganga and Brahmaputra rivers. We found that more than half of disasters are associated with monsoon LPS. Furthermore, the disasters associated with monsoon depressions are more frequent and geographically widespread, with stronger precipitation, as compared to the disasters associated with monsoon lows. Although LPS occur somewhat frequently, with around 15 forming each summer over South Asia, their association with disasters is stronger than what would occur by chance. Specifically, the relative risk of a disaster occurring when an LPS is present within 800 km of a location is larger than 1 in most of our domain, with relative risk exceeding 10 in many regions.

We found that disasters occur mostly along the northern edge of the main cluster of LPS tracks, while peak rainfall in LPS is well-known to lie southwest of the LPS centre. We confirmed this location of peak rainfall in our track dataset (Supplementary Fig. 1), so this discrepancy is not caused by anomalous behaviour of the LPS in our dataset. Given that geomorphology, fluvial transport, and groundwater hydrology all control how precipitation is related to flood characteristics, it is not surprising that there is a spatial offset between the peak LPS rainfall and the disaster location. Furthermore, we illustrated how human exposure may contribute to such offsets, with the peak population density located hundreds of kilometres to the north of the peak precipitation in a storm-centred composite of LPS (Supplementary Fig. 2).

Observations obtained from GPM show a sharp peak in rainfall on the day of disasters. This peak is more prominent for disasters associated with LPS than for non-LPS disasters, which suggests a physical link between LPS and hydro-meteorological disasters. Numerical weather prediction model forecasts also show a similar peak in precipitation for disasters associated with LPS. This peak is clearly visible for forecasts made even up to five days before disasters, although the peak rainfall decreases with increasing forecast lead time. These short-term forecasts of LPS tracks and precipitation might thus be useful in designing disaster early warning systems and in improving disaster preparedness.

Although it was not a focus of our analysis, we briefly examine the occurrence of fatalities in LPS-associated disasters. The mean number of fatalities in disasters associated with monsoon depressions is higher than that in disasters associated with lows (Supplementary Fig. 5), but the uncertainties are large enough that these differences are not distinct when considering the 95% confidence interval of the means. A distinct difference is found between the average fatalities in disasters associated with multiple LPS and the average in single monsoon lows. This highlights the importance of considering the impacts of LPS travelling through regions that were recently traversed by another LPS, though more work is clearly needed to understand the relevance of geophysical hazards such as elevated river and

groundwater levels and the time-evolution of social vulnerability. Future work could also assess the possible influence of LPS characteristics on the severity of disasters as well as the influence of co-occuring phenomena, like the boreal summer intraseasonal oscillation (BSISO), that are thought to alter LPS and their associated precipitation[40–42].

METHODS

Datasets

Disaster information is obtained from the Emergency Events Database [EM-DAT[43]], and is then geocoded using the Wrangler for Emergency Events Database (WEED; https://github.com/cran/weed) package[44]. As our main focus is South Asia, we only consider disasters occurring in India, Pakistan, Bangladesh, Bhutan, Nepal, and Sri Lanka. We also restrict our analysis to the months of June–September, as monsoon LPS are mainly active during this summer monsoon season. EM-DAT classifies disasters into categories based on the primary triggering event; we only consider hydrological and meteorological disasters, thus excluding disasters caused by earthquakes, drought, epidemics, and other events unrelated to precipitation. A single disaster event often affects multiple locations, so here we refer to each potentially large-scale event as a "disaster event", and the constituent locations as "disaster locations". As disaster information over South Asia is more sparse in the earlier part of the twentieth century, we limit our analysis to 1990–2019. For this period, EM-DAT has about 492 disaster events, of which 67 do not have specific dates of occurrence. In addition, 81 EM-DAT disaster events have information only at the state level, preventing us from assigning a geographic location more precise than the centre of the state; we also excluded those events, leaving 344 events considered in this study. However, analyses show that including these events (by using the centroid of the state as the location) does not substantially alter our results.

Tracks of monsoon LPS are obtained from the dataset compiled by Vishnu et al.[19], which used an objective algorithm based on the TempestExtremes software[45] to optimally identify LPS tracks in five atmospheric reanalyses. Here we use LPS tracks identified in ERA5[46], the most recent reanalysis of the European Centre for Medium-Range Weather Forecasts; this is a fifth-generation reanalysis providing atmospheric state estimates at hourly and 0.25° horizontal resolution, based on four-dimensional variational assimilation of a vast amount of satellite and in situ observations. The LPS tracks were further classified as monsoon depressions and lows based on the minimum surface pressure and maximum wind speeds achieved along each track. More details regarding the tracking algorithm and LPS classification can be found in Vishnu et al.[19].

Daily mean rainfall at the locations of disasters is obtained from the Global Precipitation Measurement Mission (GPM) product, which provides high-resolution ($0.1^\circ \times 0.1^\circ$) rainfall measurements from the year 2001 onward[47]. To estimate the skill of rainfall predictions at disaster locations, we use short-term weather forecasts (e.g. at 10-day lead time) from an archive of past numerical weather prediction model output: the THORPEX Interactive Grand Global Ensemble [TIGGE[48]]. Specifically, we use the deterministic ECMWF model forecasts issued at 00 UTC each day. The forecasts are available from the year 2007 onward at a horizontal resolution of $0.1^\circ \times 0.1^\circ$. In unpublished work, we have found that the ECMWF model is able to capture about 85% of the LPS tracks identified in ERA5 and, for short lead times of <5 days, has a mean track position bias of 100–300 km, much smaller than the typical horizontal scale of these storms.

Association of disasters with LPS

A disaster location is associated with a monsoon LPS if the LPS track passes within 800 km of the disaster location anytime during the duration of the disaster. The typical horizontal scale of monsoon LPS is about 2000 km and this 800 km radius was chosen for consistency with prior work that found this value to be near optimal for attributing rainfall to LPS[21,24,49]. Here, we are further assuming that the hydro-meteorological disasters occurring within this 800 km radius are due to the precipitation associated with monsoon LPS; since our identification and tracking of LPS is based on lower-tropospheric winds and not rainfall, this allows us to test this assumption (see Section "Observed precipitation"). It should be noted that the use of a fixed radius can include contributions from non-LPS events like unrelated small-scale convective activity[21], but it can also exclude disaster events that occur far from the region of precipitation, like downstream riverine floods. However, the use of a more complex method like catchment analysis is beyond the scope of this study, and for simplicity we use a fixed radius of 800 km to associate disasters with monsoon LPS.

Usually, a single disaster event affects multiple locations. We classify a disaster event as associated with an LPS if at least 50% of its locations are individually associated with the LPS. Although this attribution fraction of 50% as well as the attribution radius of 800 km were chosen somewhat subjectively, our conclusions remain qualitatively unaffected by changes in these parameters. We varied the attribution radius from 500 to 1000 km and considered attribution fractions ranging from 1% to 100%, verifying that our results did not qualitatively change. Another caveat is that the mapping of disasters to LPS is not always unique, as some disaster events can be associated with multiple LPS tracks passing within 800 km of the disaster location. Disaster events that are associated with multiple LPS may have greater severity (e.g. Supplementary Fig. 5).

DATA AVAILABILITY

Disaster information is obtained from the Emergency Events Database (https://public.emdat.be), and is then geocoded using the Wrangler for Emergency Events Database (WEED; https://github.com/cran/weed) package. Tracks of monsoon LPS from ERA5 are available in the Zenodo repository (https://doi.org/10.5281/zenodo.3890646). GPM precipitation data is available at https://gpm.nasa.gov/data/directory. ECMWF model forecasts were downloaded from the TIGGE archive (https://apps.ecmwf.int/datasets/data/tigge).

Received: 12 October 2022; Accepted: 16 May 2023;
Published online: 27 May 2023

REFERENCES

1. Ritchie, H. & Roser, M. Natural disasters. *Our World in Data* https://ourworldindata.org/natural-disasters#citation (2014).
2. UNISDR, C. et al. The human cost of natural disasters: a global perspective (2015).
3. Gaiha, R., Hill, K., Thapa, G. & Kulkarni, V. S. Have natural disasters become deadlier? *Sustainable Economic Development* 415–444 (Elsevier, 2015).
4. Julca, A. Natural disasters with un-natural effects: Why? *J. Econ. Issues* **46**, 499–510 (2012).
5. Alexander, D. *Natural Disasters* (Routledge, 2018).
6. Kahn, M. E. The death toll from natural disasters: the role of income, geography, and institutions. *Rev. Econ. Stat.* **87**, 271–284 (2005).
7. WMO. Weather-related disasters increase over past 50 years, causing more damage but fewer deaths.*World Meteorological Organization (Press Release)*. https://public.wmo.int/en/media/press-release/weather-related-disasters-increase-over-past-50-years-causing-more-damage-fewer (2021).
8. Zhongming, Z. et al. Atlas of mortality and economic losses from weather, climate and water extremes (1970-2019). (2021).
9. Haque, C. E. Perspectives of natural disasters in East and South Asia, and the Pacific Island States: socio-economic correlates and needs assessment. *Nat. Hazards* **29**, 465–483 (2003).
10. Shrestha, M. S. & Takara, K. Impacts of floods in South Asia. *J. South Asia Disaster Study* **1**, 85–106 (2008).
11. Gaiha, R. et al. Natural Disasters in South Asia. (Australia South Asia Research Centre, The Australian National University, Canberra, 2010).

12. United Nations. *World economic and social survey 2008: overcoming economic insecurity* (United Nations. Department of Economic and Social Affairs, 2008).
13. Godbole, R. V. The composite structure of the monsoon depression. *Tellus* **29**, 25–40 (1977).
14. Hurley, J. V. & Boos, W. R. A global climatology of monsoon low-pressure systems. *Q. J. R. Meteorol. Soc.* **141**, 1049–1064 (2015).
15. Mooley, D. & Shukla, J. *Characteristics of the westward-moving summer monsoon low pressure systems over the Indian region and their relationship with the monsoon rainfall* (Centre for Ocean-Land-Atmosphere Interactions, University of Maryland, College Park, MD, USA, 1987).
16. Boos, W., Hurley, J. & Murthy, V. Adiabatic westward drift of Indian monsoon depressions. *Q. J. R. Meteorol. Soc.* **141**, 1035–1048 (2015).
17. Sikka, D. *A study on the monsoon low pressure systems over the Indian region and their relationship with drought and excess monsoon seasonal rainfall* (Center for Ocean-Land-Atmosphere Studies, 2006).
18. Ajayamohan, R., Merryfield, W. J. & Kharin, V. V. Increasing trend of synoptic activity and its relationship with extreme rain events over central India. *J. Clim.* **23**, 1004–1013 (2010).
19. Vishnu, S., Boos, W., Ullrich, P. & O'Brien, T. Assessing historical variability of South Asian monsoon lows and depressions with an optimized tracking algorithm. *J. Geophys. Res.: Atmos.* **125**, e2020JD032977 (2020).
20. Yoon, J.-H. & Chen, T.-C. Water vapor budget of the Indian monsoon depression. *Tellus A: Dyn. Meteorol. Oceanogr.* **57**, 770–782 (2005).
21. Hunt, K. M. & Fletcher, J. K. The relationship between Indian monsoon rainfall and low-pressure systems. *Clim. Dyn.* **53**, 1859–1871 (2019).
22. Fletcher, J. K., Parker, D. J., Hunt, K. M., Vishwanathan, G. & Govindankutty, M. The interaction of Indian monsoon depressions with northwesterly midlevel dry intrusions. *Mon. Weather Rev.* **146**, 679–693 (2018).
23. Houze, R., Rasmussen, K., Medina, S., Brodzik, S. & Romatschke, U. Anomalous atmospheric events leading to the summer 2010 floods in Pakistan. *Bull. Am. Meteorol. Soc.* **92**, 291–298 (2011).
24. Thomas, T. M., Bala, G. & Srinivas, V. V. Characteristics of the monsoon low pressure systems in the Indian subcontinent and the associated extreme precipitation events. *Clim. Dyn.* **56**, 1859–1878 (2021).
25. Nikumbh, A. C., Chakraborty, A., Bhat, G. & Frierson, D. M. Large-scale extreme rainfall-producing synoptic systems of the Indian summer monsoon. *Geophys. Res. Lett.* **47**, e2020GL088403 (2020).
26. Priya, S., Young, W., Hopson, T. & Avasthi, A. Flood risk assessment and forecasting for the Ganges-Brahmaputra-Meghna River basins. (World Bank, 2017).
27. Saha, K. & Chang, C. The baroclinic processes of monsoon depressions. *Mon Weather Rev.* **111**, 1506–1514 (1983).
28. Sanders, F. Quasi-geostrophic diagnosis of the monsoon depression of 5–8 july 1979. *J. Atmos. Sci.* **41**, 538–552 (1984).
29. Ologunorisa, T. E. & Abawua, M. Flood risk assessment: a review. *J. Appl. Sci. Environ. Manag.* **9**, 57–63 (2005).
30. Donner, W. & Rodríguez, H. Population composition, migration and inequality: the influence of demographic changes on disaster risk and vulnerability. *Soc. Forces* **87**, 1089–1114 (2008).
31. Marin, G. & Modica, M. Socio-economic exposure to natural disasters. *Environ. Impact Assess. Rev.* **64**, 57–66 (2017).
32. Ali, K., Bajracharya, R. M. & Koirala, H. L. A review of flood risk assessment. *Int. J. Environ. Agric. Biotechnol.* **1**, 238636 (2016).
33. Roy, S., Bose, A. & Chowdhury, I. R. Flood risk assessment using geospatial data and multi-criteria decision approach: a study from historically active flood-prone region of Himalayan foothill, India. *Arab. J. Geosci.* **14**, 1–25 (2021).
34. Andrade, C. Understanding relative risk, odds ratio, and related terms: as simple as it can get. *J. Clin. Psychiatry* **76**, 21865 (2015).
35. Morris, J. A. & Gardner, M. J. Statistics in medicine: calculating confidence intervals for relative risks (odds ratios) and standardised ratios and rates. *Brit. Med. J. (Clin. Res. ed.)* **296**, 1313 (1988).
36. Francis, P. & Gadgil, S. Intense rainfall events over the west coast of India. *Meteorol. Atmos. Phys.* **94**, 27–42 (2006).
37. Kushwaha, P., Sukhatme, J. & Nanjundiah, R. A global tropical survey of mid-tropospheric cyclones. *Mon. Weather Rev.* **149**, 2737–2753 (2021).
38. Hunt, K. M., Turner, A. G. & Parker, D. E. The spatiotemporal structure of precipitation in Indian monsoon depressions. *Q. J. the R. Meteorol. Soc.* **142**, 3195–3210 (2016).
39. Deoras, A., Hunt, K. M. & Turner, A. G. Comparison of the prediction of Indian monsoon low pressure systems by subseasonal-to-seasonal prediction models. *Weather Forecast.* **36**, 859–877 (2021).
40. Goswami, B. N., Ajayamohan, R., Xavier, P. K. & Sengupta, D. Clustering of synoptic activity by Indian summer monsoon intraseasonal oscillations. *Geophys. Res. Lett.* **30** (2003).
41. Karmakar, N., Boos, W. R. & Misra, V. Influence of intraseasonal variability on the development of monsoon depressions. *Geophys. Res. Lett.* **48**, e2020GL090425 (2021).
42. Hunt, K. M. & Turner, A. G. Non-linear intensification of monsoon low-pressure systems by the BSISO. *Weather Clim. Dyn.* **3**, 1341–1358 (2022).
43. Guha-Sapir, D., Below, R. & Hoyois, P. EM-DAT: International disaster database. *Catholic University of Louvain: Brussels, Belgium* **27**, 57–58 (2015).
44. Kripa, R. M., Ramesh, N. & Boos, W. R. Wrangler for the Emergency Events Database: a tool for geocoding and analysis of a global disaster dataset. Preprint at https://doi.org/10.48550/arXiv.2208.12634 (2022).
45. Ullrich, P. A. & Zarzycki, C. M. TempestExtremes: a framework for scale-insensitive pointwise feature tracking on unstructured grids. *Geosci. Model Dev.* **10**, 1069–1090 (2017).
46. Hersbach, H. et al. The ERA5 global reanalysis. *Q. J. R. Meteorol. Soc.* **146**, 1999–2049 (2020).
47. Huffman, G. J., Bolvin, D. T., Nelkin, E. J. & Tan, J. Integrated Multi-satellitE Retrievals for GPM (IMERG) technical documentation. *NASA/GSFC Code* **612**, 2019 (2015).
48. Bougeault, P. et al. The THORPEX interactive grand global ensemble. *Bull. Am. Meteorol. Soc.* **91**, 1059–1072 (2010).
49. Dong, W., Ming, Y. & Ramaswamy, V. Projected changes in South Asian monsoon low pressure systems. *J. Clim.* **33**, 7275–7287 (2020).

ACKNOWLEDGEMENTS

The authors thank the reviewers for their valuable comments and suggestions, which greatly improved this manuscript. The authors acknowledge financial support from the Earth System Science Organization, Ministry of Earth Sciences, Government of India (Grant IITM/MM-II/Univ_California_USA/INT-3) to conduct this research under the Monsoon Mission. The authors also acknowledge support from the U.S. Department of Energy, Office of Science, Office of Biological and Environmental Research, Climate and Environmental Sciences Division, Regional and Global Model Analysis Program, under Award DE-SC0019367. This work used resources of the National Energy Research Scientific Computing Center (NERSC), which is a DOE Office of Science User Facility.

AUTHOR CONTRIBUTIONS

D.L.S. and W.R.B. designed the study, analysed the results and wrote the initial manuscript. D.L.S. developed the methodology, conducted the data analyses and prepared the figures. R.M.K. and N.R. geocoded the disaster information. All authors were involved in interpreting the results and contributed to the final version of the manuscript.

COMPETING INTERESTS

The authors declare no competing interests.

ADDITIONAL INFORMATION

Supplementary information The online version contains supplementary material available at https://doi.org/10.1038/s41612-023-00376-5.

Correspondence and requests for materials should be addressed to D. L. Suhas.

Reprints and permission information is available at http://www.nature.com/reprints

Publisher's note Springer Nature remains neutral with regard to jurisdictional claims in published maps and institutional affiliations.

Supplementary information for Influence of monsoon low pressure systems on South Asian disasters and implications for disaster prediction

D. L. Suhas[1*], Nandini Ramesh[2], Ram M. Kripa[1] and William R. Boos[1,3]

[1]Department of Earth and Planetary Science, University of California, Berkeley.
[2]Natural Systems Modelling Group, Data61, Commonwealth Scientific and Industrial Research Organisation, Australia..
[3]Climate and Ecosystem Sciences Division, Lawrence Berkeley National Laboratory.

*Corresponding author(s). E-mail(s): suhasdl@berkeley.edu;

Supplementary Discussion

Skill of ECMWF precipitation forecasts

LPS storm-centred precipitation composites show that the ECMWF forecasts are able to capture the observed precipitation peak to the southwest of the vortex centre, but it underestimates the peak magnitude (Supplementary Figure 1). Scattered plots of spatially averaged precipitation (within 5° of the LPS centre, rather than 8°, to better capture the highest rain rates) shows the ECMWF model having issues forecasting heavy precipitation, especially for rain rates exceeding 20 mm/day (Supplementary Figure 1d). Mean skill score [1] for spatially averaged precipitation at a lead time of 72 hours reveals that the ECMWF model has about 34% additional skill in comparison to observed LPS climatology. While ECMWF forecasting skills are known to have improved over the years [2], we don't see any substantial improvements for precipitation associated with monsoon LPS. For example, the mean skill score only increased from 0.33 (for the years 2007-2012) to 0.35 (for 2013-2019). However, it should be noted that both the errors in LPS precipitation and LPS track position contributes to the biases seen in Supplementary Figure 1, and more work is needed to delineate them.

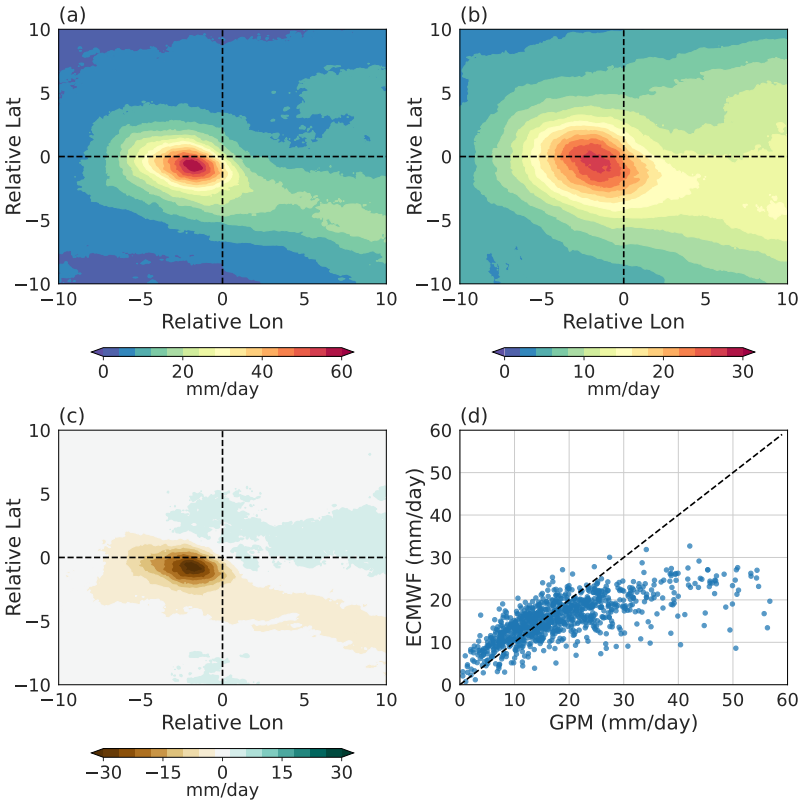

Supplementary Figure 1. Skill of ECMWF precipitation forecasts. LPS storm-centred composite mean of the (a) observed daily precipitation from GPM, (b) ECMWF forecasts and (c) bias in the ECMWF forecasts. The ECMWF forecasts are for a lead time of 72 hours. The bias is computed using precipitation data from GPM, and the LPS track locations are obtained from ERA5. Panel (d) compares precipitation forecasts by the ECMWF model with the GPM data, with precipitation averaged over a 5° region around the centre of the LPS. The plots are for the years 2007–2019.

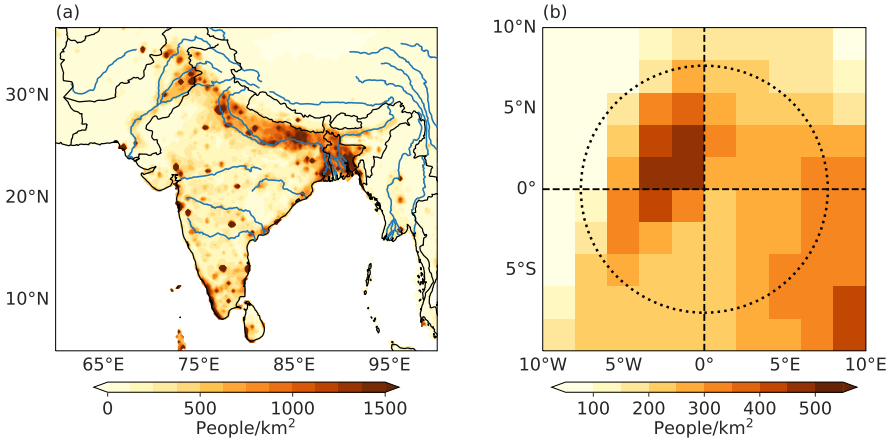

Supplementary Figure 2. Population exposure to monsoon LPS. (a) Spatial distribution and (b) LPS storm-centred composite of population density. Population density is for the year 2005, which is the mid-point of the period considered in this study (1990-2019). For the LPS storm-centred composite, all LPS tracks were considered regardless of the occurrence of disasters. Population density data is obtained from NASA's Socioeconomic Data and Applications Center (SEDAC).

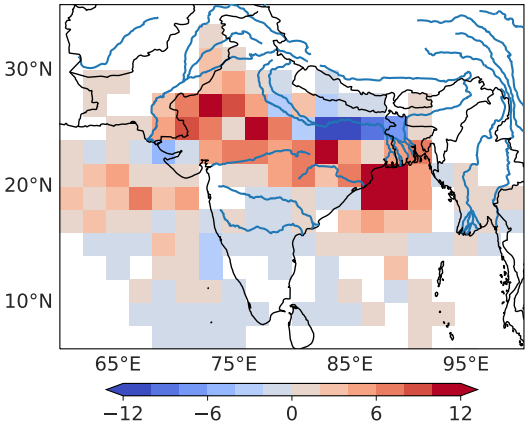

Supplementary Figure 3. Differing track locations of monsoon depressions and lows. Figure shows the difference in track density between monsoon depressions and lows. Track density refers to the annual mean number of depressions or lows seen in each $2° \times 2°$ box, and is calculated for June to September of 1990–2019.

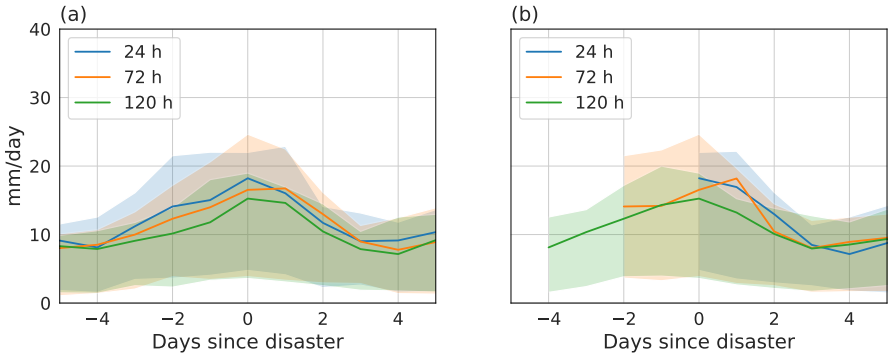

Supplementary Figure 4. ECMWF precipitation forecasts for disasters not associated with LPS. Time series of ECMWF model forecast daily rainfall at the disaster location for disaster events not associated with LPS, (a) for forecasts made 24 hours, 72 hours, and 120 hours before each day in the time series, and (b) for forecasts made 24 hours, 72 hours, and 120 hours before the day of the disaster. Day 0 corresponds to the day the disaster occurs. The shading encompasses the 25th and 75th percentiles. The plots are for the years 2007–2019.

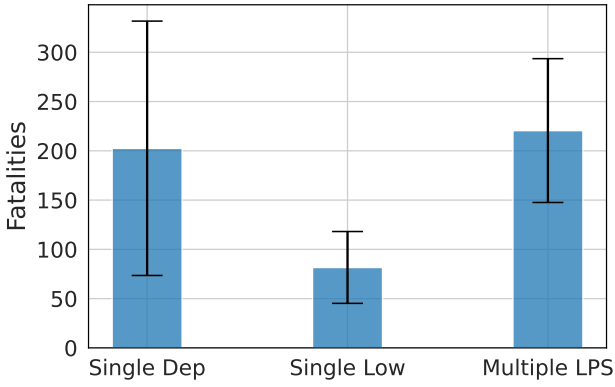

Supplementary Figure 5. Fatalities associated with disaster events. Average fatalities per disaster event, with disasters stratified by the strength and number of LPS associated with each disaster. Fatalities from disasters associated with only a single depression, only a single low, and with multiple LPS are shown. Means are shown by blue horizontal bars, while error bars mark the 95% confidence interval for the mean. Only the difference in mean fatalities for disasters associated with a single low and multiple LPS systems is statistically significant, evaluated using a t-test at a 95% confidence level. The plots are for the years 1990–2019.

Supplementary References

[1] Wilks, D. S. *Statistical methods in the atmospheric sciences* Vol. 100 (Academic press, 2011).

[2] Forbes, R., Haiden, T. & Magnusson, L. Improvements in IFS forecasts of heavy precipitation. *ECMWF Newsletter* **144**, 21–26 (2015) .